Electrochemical, EPR, and Magnetic Studies on Microcrystals of the $[C_{60}\subset(p\text{-Benzyl-calix[5]arene})_2]\bullet 8$Toluene and Its One-Electron-Reduced Encapsulation Complex

Alan M. Bond,* Wujian Miao, Colin L. Raston, and Christian A. Sandoval

Department of Chemistry, Monash University, Clayton, Victoria 3800, Australia

Received: May 11, 2000

The electrochemical behavior of microcrystals of the $[C_{60}\subset(p\text{-benzyl-calix[5]arene})_2]\bullet 8$toluene (referred to as $C_{60}\subset L_2$) encapsulation complex adhered to electrode surfaces in contact with CH_3CN (electrolyte) has been studied using cyclic voltammetric and microgravimetric techniques. Six successive one-electron reduction processes, of which the first two have chemically reversible characteristics, are observed at a glassy carbon electrode when large Bu_4N^+ cations are used as the electrolyte, although dissolution of the reduced solid into the bulk solution also accompanies the reduction processes. Under the same conditions but with an electrolyte containing much smaller Li^+, Na^+, or Ba^{2+} cations, all reduction processes were found to be chemically irreversible. These chemically reversible/irreversible reduction processes are attributed to the reversible/irreversible intercalation processes of large/small electrolyte cations into the lattice of $C_{60}\subset L_2$ crystals. In EPR studies, the *g* values of 2.0020 ± 0.0002 at 293 K and 2.0022 ± 0.0002 at 77 K found for reduced solid $[C_{60}\subset L_2]^{\bullet -}$ containing Ba^{2+} cations suggest that significant fullerene structure distortion is present in this one-electron-reduced form of solid. Magnetic measurements indicated that extensive unpaired electron delocalization may occur within the structure of this reduced $[C_{60}\subset L_2]^{\bullet -}$ solid and that the reduced solid is relatively stable in air. Data show that the interactions between C_{60} and the calix[5]arene to form an encapsulation complex are sufficiently strong that free one-electron-reduced C_{60} anions are not produced even during the course of reduction, as is the case with previously studied C_{60} host−guest complexes.

Introduction

Calixarenes (Figure 1), a group of polyphenolic bowl/basket-shaped molecules with hydrophobic cavities, have been shown to form a number of discrete host−guest complexes with fullerene C_{60}.[1−12] Such interactions are of interest in direct purification of fullerenes from carbon soot,[3,4,13,14] in biological applications[15,16] and in material science.[15] Recently, the electrochemical behavior of calixarene-C_{60} complexes has been reported.[5,17−19] Chen et al.[5] used cyclic and square wave voltammetry to study the complexation of C_{60} by titrating amounts of calix[4, 5, and 8]arenes into a solution of C_{60} and observed the reduction processes associated with the complexes formed in situ. Bond et al.[19] reported the cyclic voltammetry of C_{60} and electron paramagnetic resonance (EPR) spectroscopy of $C_{60}^{\bullet -}$ in the presence of calix[5]arene (Figure 1a, R = H, $n = 5$) and related bowl-shaped cyclotriveratrylene complexing agents. It was shown that the first four initial reduction potentials of C_{60} were perturbed on complexation and formation of host−guest $\pi-\pi$ interactions and that they were sufficiently strong to affect the EPR signals of $C_{60}^{\bullet -}$. Bard et al.[18] have recently studied the electrochemical reduction of solid *p-tert*-butyl-calix[8]arene-C_{60} "films" in CH_3CN using K^+, Bu_4N^+, and $Zn(bpy)_3^{2+}$ as electrolytes through a combination of electrochemical microscopy with an electrochemical quartz crystal microbalance technique. They found that, whereas complexation of the fullerene within the film resulted in a negative shift in the peak potential of the first reduction wave relative to the reduction of a pure C_{60} film, the complex broke apart upon reduction, with the fullerene anions escaping from the calixarene basket into the CH_3CN solution. This is consistent with the proposed micelle-like structure for the complex in which three C_{60} molecules are shrouded by three calix[8]arenes in the double-cone conformation.[20]

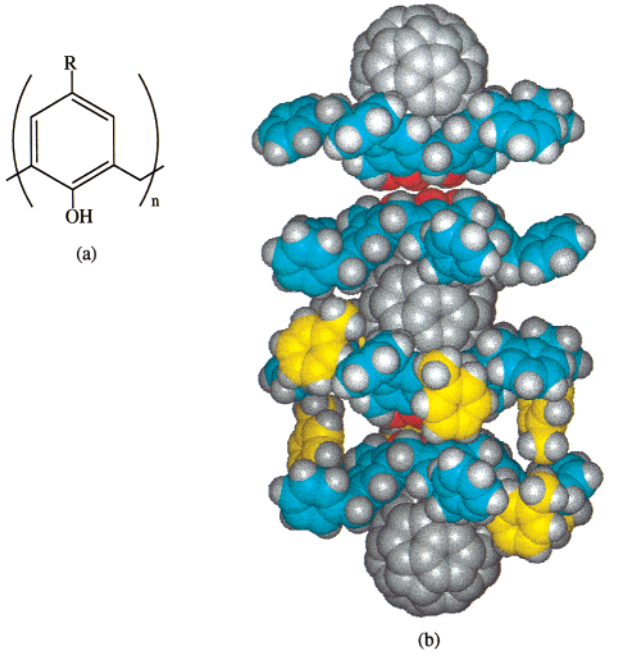

Figure 1. (a) Structure of calix[*n*]arene. (b) Columnar solid-state structural representation of successive $[C_{60}\subset(p\text{-benzyl-calix[5]arene})_2]\bullet$8toluene units. For clarity, the toluene molecules are shown for only half of the column.

* Correspondence to: Prof. Alan M. Bond. Telephone: (+613) 9905 1338. Fax: (+613) 9905 4597. E-mail: a.bond@sci.monash.edu.au.

10.1021/jp0017442 CCC: $19.00
Published on Web 08/09/2000

In contrast to the situation that prevails with *p-tert*-butylcalix[8]arene, C_{60} forms a 1:1 inclusion complex with *p*-benzylcalix[5]arene (Figure 1a, R = $C_6H_5CH_2$, $n = 5$) in toluene solution[9,12] and a 2:1 encapsulation complex in the solid state.[12] The latter crystallizes as the octa-toluene solvate, [$C_{60}\subset$(*p*-benzyl-calix[5]arene)$_2$]•8toluene (Figure 1b), which for convenience is now referred to as $C_{60}\subset L_2$. In this solid-state structure, two calixarenes are bound to a single fullerene in a trans arrangement, and the supermolecules are stacked back-to-back, with the closest intercalixarene O···O distance being 3.10 Å at −100 °C.[12]

In view of the unusual solid-state structure of $C_{60}\subset L_2$, in which the fullerene is encapsulated, reduced forms of the solid complex may be more stable than would be the case for other systems studied to date. Thus, with $C_{60}\subset L_2$, decomposition may not occur after electroreduction, as is the case with the *tert*-butyl-calix[8]arene-C_{60} complex,[18] because the reduced C_{60} anions are more likely to remain trapped within the cavities of the two calix[5]arenes, and for the calix[8]arene complex, there would be little electrostatic repulsion between the fullerenes in the micelle-like aggregate. This implies that the electrochemistry of the complex could be significantly different from that of other C_{60} complexes, and that EPR, magnetic, and other data on more stable reduced forms of the complex could be accessible. Novel features may accompany reduction because most of the surface of the fullerene is shrouded by two *p*-benzyl-calix[5]arene molecules.[12] However, the size of the cation incorporated from the supporting electrolyte in order to achieve charge neutrality in the reduced form of $[C_{60}\subset L_2]^-$ may have significant influences on the electrochemical behavior, as the space available for the cation is limited if no major structural changes occur upon reduction.

To establish whether the electrochemical behavior of $C_{60}\subset L_2$ in the solid, microcrystalline $C_{60}\subset L_2$ complex is inherently different from that of other systems, the encapsulation complex was initially adhered to the surface of a working electrode, which was then placed in contact with acetonitrile (electrolyte) solutions, in which the calixarene, C_{60}, and the complex are insoluble or only sparingly soluble.[21−27] Bu_4N^+, Li^+, Na^+, and Ba^{2+} perchlorate salts were used as supporting electrolytes. Mass changes associated with ion incorporation or dissolution reactions on the electrode surfaces during the course of redox processes were monitored by using a quartz crystal microbalance. Finally, the X-ray powder patterns and the microanalysis, EPR, and magnetic data for the one-electron reduced solid were obtained and used to confirm the hypotheses formed on the basis of voltammetric and microgravimetric data.

Experimental Section

Chemicals. The acetonitrile, C_{60}, and *n*-Bu_4NClO_4 used were as in the previous report.[28] $LiClO_4$ (PCR, Gainesville, FL), $NaClO_4$ (Ajax, Auburn, NSW, Australia) and $Ba(ClO_4)_2$ (Sigma, St. Louis, MO) were of analytical purity grade and were dried at 100 °C under N_2 for 12 h prior to use. Crystalline $C_{60}\subset L_2$ complex was prepared from a toluene solution of *p*-benzyl-calix[5]arene with C_{60} (1:1 in molar ratio). On heating, the characteristic magenta color of C_{60} dissolved in the solution changed to red, and crystals slowly precipitated on cooling. Further details on the preparation and characterization of this complex are available in the literature.[9,12]

Instrumentation and Electrodes. Cyclic voltammetric experiments were undertaken with a Cypress Systems CS-2000 computerized instrument, using a 0.10 cm diameter glassy carbon as the working electrode. Double-potential-step and quartz crystal microbalance experiments were performed with an Elchema EQCN-701 electrochemical quartz crystal nanobalance (Potsdam, New York), with 10-MHz gold-coated AT-cut quartz crystals (Bright Star Crystals, Vic, Australia) being used as the working electrodes. Mass changes accompanying electrode processes at the gold electrodes were calibrated via the electrodeposition of copper from a 1.00×10^{-3} mol L^{-1} Cu$(ClO_4)_2$ (0.10 $HClO_4$) solution with the assumption that the Sauerbery equation is valid, which requires that frequency changes associated with viscosity, pressure, and other film properties are negligible. The quartz-crystal and gold electrodes had diameters of 1.20 and 0.50 cm, respectively. With both forms of instrumentation, Pt gauze and Ag/Ag^+ (0.010 mol L^{-1} $AgNO_3$ and 0.10 mol L^{-1} Bu_4NClO_4 in CH_3CN) were used as the counter and reference electrodes, respectively. The reversible half-wave potential of ferrocene/ferricinium couple was 0.082 V vs Ag/Ag^+ in CH_3CN (0.10 mol L^{-1} Bu_4NClO_4) solutions, when ferrocene was added as an internal potential standard.

Ground microcrystalline $C_{60}\subset L_2$ complex and C_{60} (1−10 μm in diameter) were mechanically attached to the working electrode surface by using a cotton bud and rubbing a small amount of the solid gently onto the electrode. Before electroactive materials were attached, the glassy carbon electrode was polished by using a 0.3-μm Al_2O_3 (Buehler, Lake Bluff, IL) slurry, followed by washing with distilled water, acetone, and acetonitrile. Any residual solvent remaining on the electrode surface was wiped off with tissues.

Unless otherwise stated, electrochemical experiments were conducted under ambient temperature conditions of 20 ± 2 °C, and the electrolyte solutions (10 mL in cyclic voltammetry and 25 mL in quartz-crystal microgravimetry) were degassed with high purity N_2 for 5 min before the commencement of each experiment.

Bulk controlled potential electrolysis of solid $C_{60}\subset L_2$ complex was carried out using a BAS-100 Electrochemical Analyzer, with a two-compartment electrolytic cell,[29] in which the counter and working electrodes, platinum mesh, and glassy carbon cylinder were separated by a sintered glass frit. About 50 mg of solid $C_{60}\subset L_2$ complex and ∼10 mL of 0.10 mol L^{-1} Ba$(ClO_4)_2$/CH_3CN electrolyte solution were transferred into the working electrode compartment. The electrolyte solution was deoxygenated with solvent-saturated high-purity argon prior to and during electrolysis. The electroreduction potential, which was determined by cyclic voltammetric experiments, was set at −1.200 V vs Ag/Ag^+, and the bulk electrolysis was continued for ca. 10 h until the final current was 0.10% of the initial value. The reduced solid complex was immediately transferred under an argon atmosphere into an EPR tube for spectroscopic and other forms of characterization. To minimize the possible influence of oxygen, the EPR tube was kept in liquid nitrogen.

X-band EPR spectra were recorded on a Varian E−12 spectrometer at room temperature and at 77 K, with the modulation frequency set at 100 kHz and the microwave power at 1.0 mW. g values were measured versus DPPH (α,α'-diphenyl-β-picrylhydrazyl, $g = 2.0037 \pm 0.0002$), which was used as the external reference. The error in the reported g values is on the order of ±0.0002.

Magnetic susceptibility and magnetization measurements were made using a Quantum Design MPMS5 SQUID magnetometer. Samples were contained within either gelatine capsules or quartz tubes.

X-ray powder diffraction and energy-dispersive X-ray microanalysis experiments were undertaken using a PAD 5 Scintag high-resolution diffractometer and a Hitachi S-2300 scanning

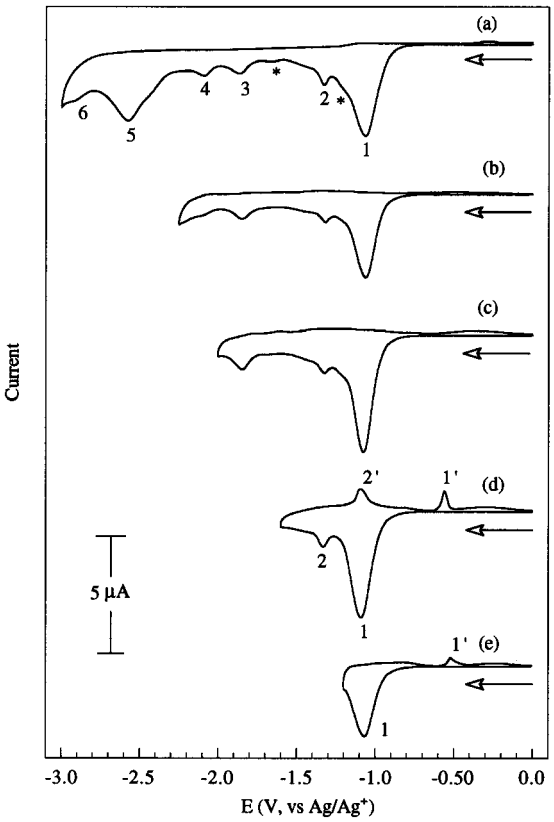

Figure 2. Cyclic voltammograms obtained over different potential ranges at a scan rate of 0.020 V s^{-1} for reduction of microcrystalline C_{60}⊂L_2 complex adhered to a 0.10 cm diameter glassy carbon electrode placed in CH_3CN (0.10 mol L^{-1} Bu_4NClO_4): (a) 0.000 to −3.000 V; (b) 0.000 to −2.250 V; (c) 0.000 to −2.000 V; (d) 0.000 to −1.600 V, and (e) 0.000 to −1.200 V vs Ag/Ag^+.

electron microscope, respectively. The solid $[C_{60}⊂L_2]^{\bullet-}$ species generated by bulk electrolysis was washed thoroughly with CH_3CN before the microanalysis determinations in order to remove adventitious electrolyte.

Results and Discussion

Cyclic Voltammetry of Solid C_{60}⊂L_2 Complex in Contact with Acetonitrile Containing the Bu_4N^+ Cation in the Electrolyte. Cyclic voltammograms obtained over different potential ranges at a scan rate of 0.020 V s^{-1} for the reduction of solid C_{60}⊂L_2 complex adhered to a glassy carbon electrode placed in CH_3CN (0.10 mol L^{-1} Bu_4NClO_4) are shown in Figure 2. Six main reduction processes, labeled as 1−6 in Figure 2a, are observed when the potential is switched at very negative values, with the peak heights for processes 1 and 5 being significantly larger than those for the others. No significant oxidation responses were detected on the reverse scans of cyclic voltammograms when potentials were switched at values more negative than that of the third reduction process (Figure 2a−c). Increasing the scan rate to 1.00 V s^{-1} had no effect on the chemical reversibility of processes 3−6, suggesting that the absence of oxidation waves on the reverse scans is a result of three-electron-reduced material being dissolved rapidly from the electrode surface and diffusing into the bulk solution phase. In contrast, when the potential is switched after either the first or the second reduction process, then on the reverse scan, the corresponding reversible couples (processes 1, 1′ and 2, 2′) are observed (Figure 2d and e), although, even in this case, the peak heights of processes 1′ and 2′ are much smaller than those of 1 and 2, as expected if some dissolution accompanies these reduction steps.

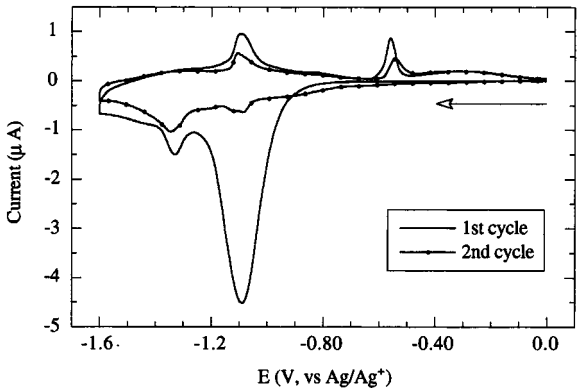

Figure 3. Effect of cycling of the potential over the first two redox processes on peak heights for reduction of microcrystalline C_{60}⊂L_2 complex adhered to a 0.10 cm diameter glassy carbon electrode placed in CH_3CN (0.10 mol L^{-1} Bu_4NClO_4) at a scan rate of 0.020 V s^{-1}.

Because the calix[5]arene and toluene molecules in crystals of the C_{60}⊂L_2 complex are electro-inactive within the range of the potential window examined and because solid C_{60} itself has been shown to be reduced to C_{60}^{6-} under experimental conditions[28] similar to those described in this study, the six reduction processes associated with solid C_{60}⊂L_2 are likely to represent consecutive one-electron-transfer reactions of complexed C_{60}. In contrast to the stable voltammetric behavior established when solid C_{60}[28,30] is reduced to almost insoluble solid C_{60}^- and C_{60}^{2-} on repetitive cycling of the potential, continuous scanning over the first pair of waves, or over both the first and second pairs, ultimately leads to the almost complete disappearance of both processes, with a particularly significant decrease in peak heights being observed during the course of the second potential cycle (Figure 3). This suggests that the one-electron- and two-electron-reduced complex calixarene species, unlike C_{60}^- and C_{60}^{2-}, are not able to form stable insoluble films with Bu_4N^+ cations obtained from the electrolyte in CH_3CN and that, upon the electroreduction, even the one- and two-electron-reduced materials initially attached to the electrode slowly dissolve from the surface of the electrode and diffuse into the bulk of the solution.

The hypothesis of dissolution of the reduced form of the complex is consistent with data obtained from the electrochemical quartz crystal microbalance (EQCM) experiments at a gold electrode. Differences between cyclic voltammograms obtained for glassy carbon and gold electrodes are relatively minor, so the EQCM data obtained at a gold electrode surface is believed to also apply to that shown above at the glassy carbon surface. Figure 4 shows an example of the simultaneous cyclic voltammetric and EQCM gravimetric responses for the reduction of solid C_{60}⊂L_2 complex adhered onto a Au/QC electrode placed in contact with CH_3CN (0.10 mol L^{-1} Bu_4NClO_4). Clearly, very little change in mass is observed prior to the potential reaching a value where the initial electroreduction occurs. However, a rapid loss in mass accompanies the first reduction process, and a further decrease in mass is associated with the second reduction process. It is evident that all solid is lost from the Au/QC electrode after process 3, because no mass change is observed after reduction process 3 has been passed. Thus, only the first two, and possibly the third, reduction processes are generated from reduction of surface-attached solid-state complexes, whereas processes 4−6 are produced by reduction of dissolved solution-phase species. The dramatic decrease in peak heights of processes 2−4 in Figures 2 and 4 relative to that of process 1 are, therefore, assigned predominantly to the progressive loss of solid from the electrode surface. The minor waves between main reduction peaks (indicated by "*" in Figures 2a

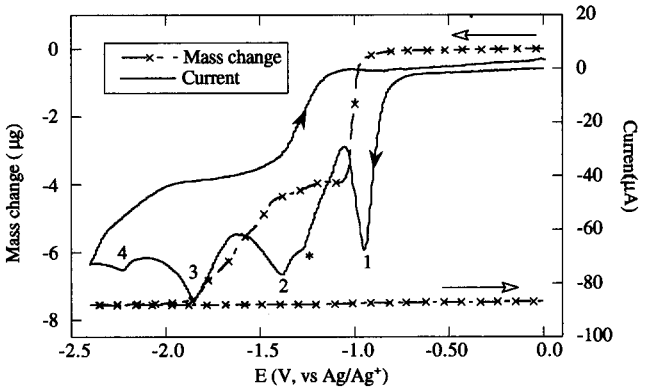

Figure 4. Cyclic voltammograms (−) with mass changes (−x−x−) obtained at a scan rate of 0.020 V s^{-1} for reduction of microcrystalline $C_{60}\subset L_2$ complex adhered to a 0.50 cm diameter Au/QC electrode placed in CH_3CN (0.10 mol L^{-1} Bu_4NClO_4).

and 4) are believed to be associated with the diffusion and/or diffusion−reduction−adsorption processes of dissolved species. Data in Figure 4 obtained at very negative potentials, therefore, also establish that, in the particular experiment displayed, about 7.5 μg of solid are attached initially to the electrode surface in these Au/QC electrode experiments. On the basis of repetitive experiments, it was shown that the mass present on an electrode was 7.5 ± 0.2 μg, but irrespective of the initial value, the same trend was observed in each experiment. This mass is of the same order of magnitude as that used for analogous C_{60} experiments in dichloromethane in which both C_{60} and C_{60}^- can both be dissolved from the electrode surface.[31]

The above discussion explains why process 1 has a relatively large peak current. The reason for the relatively large peak 5 current almost certainly has a different origin. Previously,[28,32] it was established that the presence of traces of water can significantly enlarge the peak current for solution-phase $C_{60}^{5-/6-}$ reduction process in CH_3CN (0.10 mol L^{-1} Bu_4NClO_4), because multiple electron transfers and coupled protonation reactions are induced under these circumstances. The enhancement of the peak height for process 5 shown in Figure 2a during the reduction of solid $C_{60}\subset L_2$ complex also can be attributed to this kind of mechanism. In support of this hypothesis it was shown that, under dry conditions (CH_3CN passed through an activated alumina column several times, extensively dried Bu_4NClO_4 electrolyte, and carefully dried glassy carbon electrodes), the peak height for the fifth reduction of the solid $C_{60}\subset L_2$ complex is significantly reduced. In contrast, after traces of water are deliberately added or after the acetonitrile (electrolyte) solution is allowed to stand in the air for ca. 30 min, the peak heights for the fifth and the sixth reduction processes are significantly increased.

Cyclic Voltammetry of Solid $C_{60}\subset L_2$ Complex and Solid C_{60} in the Presence of Li^+, Na^+, and Ba^{2+} Electrolytes. In CH_3CN and with Li^+ as an electrolyte, cyclic voltammograms of the solid $C_{60}\subset L_2$ complex showed an initial reduction process (process 1 in Figure 5a1), followed by a broad reduction region (reduction region 2, Figure 5a1) that clearly consists of a series of unresolved processes. Analogous behavior also was observed in the presence of a Na^+ electrolyte (Figure 5b1). However, only the first reduction process is well-defined in the presence of Ba^{2+} (Figure 5c). In contrast to the voltammetric responses of surface-attached solid $C_{60}\subset L_2$ complex in contact with acetonitrile containing Bu_4N^+ electrolyte (Figure 2e), after the potential was switched after process 1, no oxidation wave was observed on the reverse scan, regardless of whether Li^+, Na^+, or Ba^{2+} was used as the electrolyte cation (Figure 5a2, b2, and

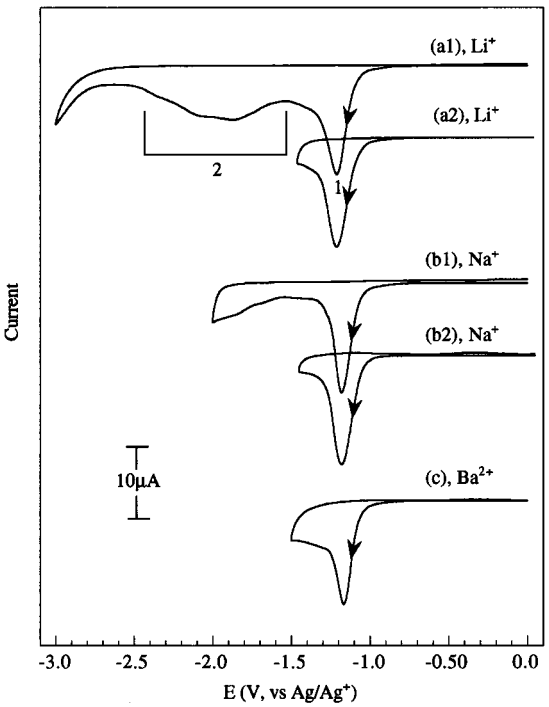

Figure 5. Cyclic voltammograms obtained over different potential ranges at a scan rate of 0.100 V s^{-1} for reduction of microcrystalline $C_{60}\subset L_2$ complex adhered to a 0.10 cm diameter glassy carbon electrode placed in CH_3CN containing different electrolytes: (a1) 0.000 to −3.000 V and (a2) 0.000 to −1.500 V in 0.10 mol L^{-1} $LiClO_4$, (b1) 0.000 to −2.000 V and (b2) 0.000 to −1.500 V in 0.10 mol L^{-1} $NaClO_4$, and (c) 0.000 to −1.500 V vs Ag/Ag^+ in 0.10 mol L^{-1} $Ba(ClO_4)_2$.

c) and regardless of the scan rate (0.020−1.00 V s^{-1}). This behavior was unchanged even when the positive potential direction scan encompassed values close to +1.0 V vs Ag/Ag^+, at which point the calix[5]arene ligand starts to oxidize.

Under the same experimental conditions, but with solid C_{60} rather than $C_{60}\subset L_2$ mechanically attached to a glassy carbon electrode, six successive one-electron-transfer processes are observed (Figure 6a2) upon electroreduction in the presence of 0.10 mol L^{-1} $LiClO_4$ electrolyte, with peak potential values of −1.26, −1.71, −1.86, −2.08, −2.74, and −3.13 V vs Ag/Ag^+ at a scan rate of 0.100 V s^{-1}. Again, the sixth relatively large reduction peak is attributed to the occurrence of multiple electron transfer and protonation processes, which occur with highly reduced forms of solid C_{60}[28] and $C_{60}\subset L_2$ complex (see above) adhered to electrodes that are in contact with CH_3CN when Bu_4NClO_4 was used as the electrolyte. When the potential was cycled between 0.000 and −1.500 V vs Ag/Ag^+, a pair of small waves preceded major process 1 in the presence of Li^+, Na^+, and Ba^{2+} electrolyte solutions (Figure 6a3, b, and c). These results obtained with microcrystals of C_{60} are consistent with the data obtained for the reduction of C_{60} films.[33,34]

Comparison of the Cyclic Voltammetry Results Obtained with Solid $C_{60}\subset L_2$ Complex and C_{60}. A comparison of the cyclic voltammograms obtained for the reduction of solid $C_{60}\subset L_2$ complex (Figures 2, 3, and 5) and solid C_{60} (Figure 6 and ref 28) implies that no significant amount of free C_{60} anions are generated at any level of reduction of the solid $C_{60}\subset L_2$ complex under the experimental conditions of our studies. That is, reduced C_{60} anions always remain trapped within the cavities of the *p*-benzyl-calix[5]arene, unlike the case with other C_{60} calixarene combinations.[12] This implies that the $\pi-\pi$ and $\sigma-\pi$ interactions between C_{60} and the two calix[5]arene molecules are sufficiently strong to overcome the impact caused by the

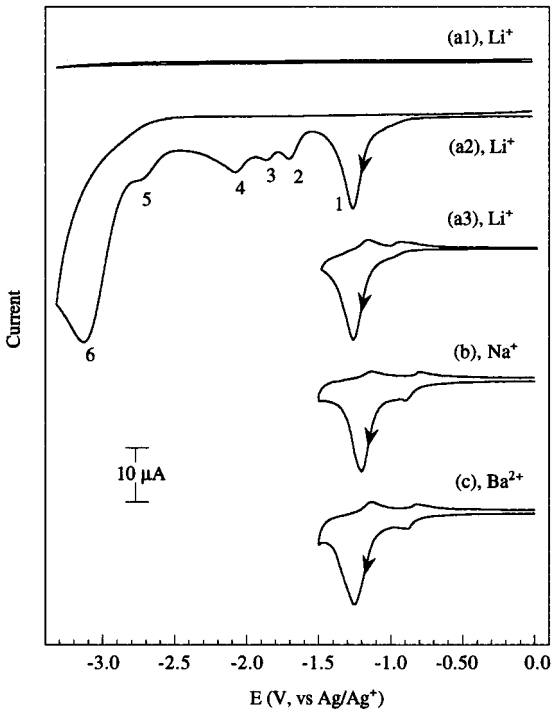

Figure 6. Cyclic voltammograms obtained at a scan rate of 0.100 V s^{-1} for reduction of microcrystalline C_{60} adhered to a 0.10-cm-diameter glassy carbon electrode placed in CH_3CN with different electrolytes. The baseline is shown in curve a1. Electrolyte concentrations, 0.10 mol L^{-1}.

TABLE 1: Comparison of the Reduction Peak Potentials for the C_{60}⊂L_2 Complex (E_p^a) and C_{60} (E_p^b) Adhered to a 0.10-cm-Diameter Glassy Carbon Electrode Placed in CH_3CN Containing 0.10 Mol L^{-1} of Electrolyte[a]

reduction process	electrolyte cation	E_p^a, V C_{60}⊂L_2	E_p^b, V C_{60}	ΔE_p, mV ($E_p^a - E_p^b$)
1	Bu_4N^+	−1.17	−1.21	+40
2		−1.33	−1.25	−80
3		−1.87	−1.76	−110
4		−2.12	−2.06	−60
5		−2.65	−2.61	−40
1	Li^+	−1.21	−1.26	+50
1	Na^+	−1.18	−1.20	+20
1	Ba^{2+}	−1.17	−1.25	+80

[a] *E* vs Ag/Ag^+, scan rate = 0.100 V s^{-1}.

additional electron density added to the complex during the course of reduction processes. The large contact area and the C_5 symmetry matching between the fullerene and the two *p*-benzyl-calix[5]arene ligands[12] are postulated to play an important role in the stabilization of the reduced solid.

Table 1 lists the reduction peak potentials of both the solid C_{60}⊂L_2 complex and solid C_{60} adhered to a glassy carbon electrode placed in contact with CH_3CN containing different electrolytes at a scan rate of 0.100 V s^{-1}. The first reduction processes of the C_{60}⊂L_2 complex occur at less negative potential values by 20−80 mV relative to the reduction of solid C_{60}, and the second to sixth peak potential values are shifted negatively by 40−110 mV relative to those of solid C_{60}. Under the related experimental conditions, but with films rather than microcrystals, complexation of the fullerene with *p-tert*-butyl-calix[8]arene, results in a negative shift in the peak potential of the first reduction wave by about 400 mV relative to that for the reduction of a pure C_{60} film.[18]

Influence of Electrolyte Cation Size on the First Solid-State C_{60}⊂L_2 Reduction Process. Two classes of voltammetric behavior are observed in the electrochemical reduction of solid C_{60}⊂L_2 complex in the potential region corresponding to the first process. The large tetrabutylammonium Bu_4N^+ cation, which has a size similar to that of C_{60}, notably 10 Å in diameter,[34,35] gives the chemically reversible class of response, whereas the much smaller Li^+, Na^+, and Ba^{2+} metal cations give a distinctly different class of irreversible voltammetric response. The diameter of the metal cations is between 1.2 and 2.7 Å,[36] which is less than the closest intercalixarene O···O distance of 3.10 Å in C_{60}⊂L_2.[12] As shown in Figures 2e and 5, voltammograms of the solid C_{60}⊂L_2 complex include a chemically reversible one-electron redox process when the large Bu_4N^+ cation is present in the electrolyte, whereas a completely irreversible initial reduction process is observed when small metal cations are used as the electrolyte. This distinctly different behavior with respect to chemical irreversibility is readily explained on the basis of the C_{60}⊂L_2 complex structure (Figure 1b). When the complex is reduced, it obtains an overall negative charge so that some electrolyte cations must be transported from the solvent (electrolyte) phase into the matrix of the crystals in order that charge balance be achieved. The smaller size of Li^+, Na^+, and Ba^{2+} cations makes them suitable to fit into the central spaces between two calix[5]arenes without requiring any major structural change in the crystals. The electron density is much higher in this central region than elsewhere, because of the existence of 10 phenol −OH groups, and once incorporated, cations remain even after the potential direction is switched and scanned positively to +1.0 V vs Ag/Ag^+. In contrast, the Bu_4N^+ cation is much too large to completely fit into the central space, so it can more readily leave the structure. Thus, a reversible intercalation process involving Bu_4N^+ cations can readily occur over a narrow potential range and give rise to both reduction and oxidation of the solid C_{60}⊂L_2 complex on the surface of the electrode. Of course, toluene molecules initially present in the crystals of the complex may diffuse out of the solid prior to and/or during the course of the reduction process in order to provide any additional space requirements for cations.

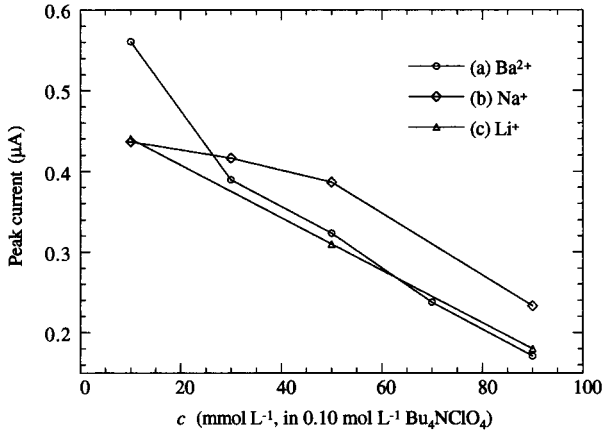

Figure 7. Effect of the concentration of Li^+, Na^+, and Ba^{2+} cations added to a 0.10 mol L^{-1} Bu_4NClO_4 acetonitrile solution on the oxidation peak current of microcrystalline C_{60}⊂L_2 complex adhered to a 0.10-cm-diameter glassy carbon electrode. Potential range, 0.000 to −1.300 V (Li^+ and Ba^{2+} media) or 0.000 to −1.200 V vs Ag/Ag^+. Scan rate, 0.020 V s^{-1}. (Na^+ media, $i_p/3.0$.)

The magnitude of the reoxidation current on the cyclic voltammogram obtained for the reduction of solid C_{60}⊂L_2 complex (process 1′ in Figure 2e) was decreased after the addition of small amounts of Li^+, Na^+, or Ba^{2+} cations to a 0.10 mol L^{-1} Bu_4NClO_4 acetonitrile solution (Figure 7). This result further supports the concept that electrochemically induced intercalation of small cations into the reduced crystals is the

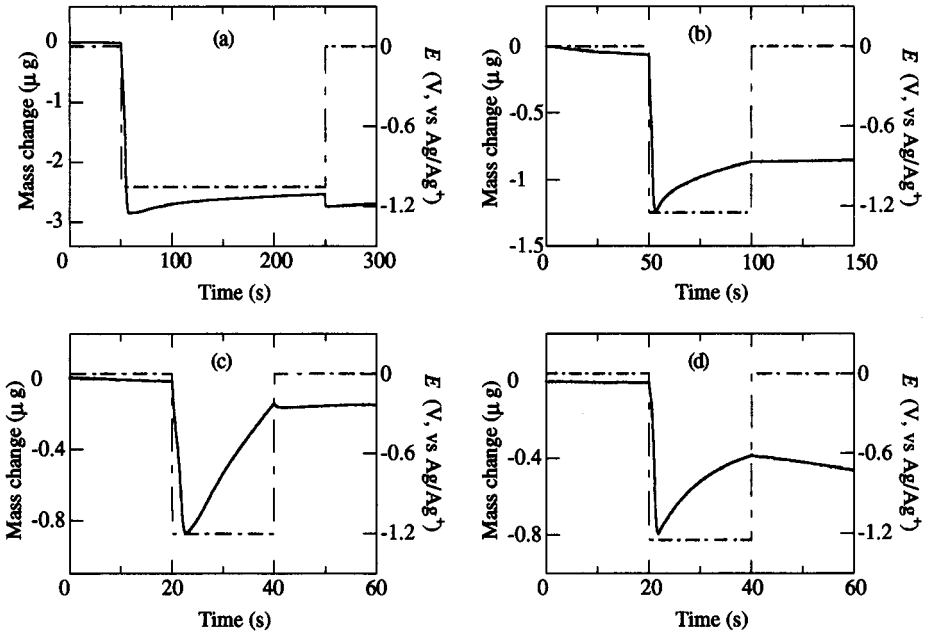

Figure 8. EQCM−double-potential-step experiments on microcrystalline $C_{60}\subset L_2$ adhered to a 0.50-cm-diameter Au/QC electrode placed in CH_3CN containing 0.10 mol L^{-1} (a) Bu_4NClO_4, (b) $LiClO_4$, (c) $NaClO_4$, and (d) $Ba(ClO_4)_2$, showing mass changes (solid lines) as a function of potential (dashed lines).

origin of the irreversibility of the electrochemical process, at least within the potential region available in these studies.

Information Obtained from Microgravimetric−Double-Potential-Step (EQCM) Experiments on the Intercalation/Expulsion of Electrolyte Cations. Microgravimetric−double-potential-step experiments were performed with the EQCM technique at a gold electrode surface to monitor the mass changes when microcrystalline $C_{60}\subset L_2$ complex adhered to a Au/QC electrode placed in CH_3CN was reduced in the presence of different electrolytes. The potentials used in the double-potential-step experiments were chosen on the basis of data obtained by cyclic voltammetry at a Au/QC electrode (see, for example, Figure 4). Thus, the potential was initially held at 0.000 V vs Ag/Ag^+, where no significant reduction of solid $C_{60}\subset L_2$ complex occurred. After 20−50 s, the potential was then stepped to values of −1.050, −1.250, −1.200, or −1.250 V vs Ag/Ag^+ for electrolyte solutions containing Bu_4N^+, Li^+, Na^+, or Ba^{2+} cations, respectively, and for cases in which the complex was assumed to be rapidly reduced in a one-electron process. Finally, after an additional period of time, the potential was returned to the initial value of 0.000 V vs Ag/Ag^+, where the reduced species could be oxidized back to its original state, accompanied by the expulsion of cations from the crystal lattice, if the redox processes were chemically reversible.

As shown in Figure 8a, when the electrolyte solution contains the large Bu_4N^+ cations, the mass of the $C_{60}\subset L_2$ complex remains almost constant at the initial potential value (a very slow loss is detected), confirming that the neutral complex is almost insoluble in acetonitrile. However, after the potential is switched to −1.050 V vs Ag/Ag^+, a significant mass loss of about 3 μg is observed in the first 8 s, and then the mass gradually increases with time. Clearly, not all of the mass is lost in this early stage, as about 7.5 μg of solid was present initially on the electrode surface (Figure 4). The time dependence of the mass change suggests that, in the one-electron-reduced state, the complex rapidly loses toluene. At the same time, dissolution of some of the complex occurs to give a saturated solution, after which the rate of dissolution decreases and the mass increase resulting from incorporation of the large Bu_4N^+ cation can be detected, which results in the detection of a mass increase at longer times. Importantly, 200 s later, when the potential is stepped back to 0.000 V vs Ag/Ag^+, a sudden mass loss is observed, which is as expected if the reversible release of Bu_4N^+ cations occurs from the complex crystal lattice when the reduced solid remaining on the electrode surface is converted back to the oxidized form. This result is consistent with the model of slow dissolution coupled with a chemically reversible intercalation process, as deduced on the basis of cyclic voltammetry for the reduction of the microcrystalline $C_{60}\subset L_2$ complex at a glassy carbon electrode in 0.10 mol L^{-1} Bu_4NClO_4 electrolyte solutions of acetonitrile (see above).

Figure 8b−d display the EQCM−double-potential-step results for $C_{60}\subset L_2$ complex in CH_3CN when the smaller Li^+, Na^+, and Ba^{2+} cations are used in the electrolyte. Similar to the case for Bu_4N^+ cations, in each electrolyte solution, only a small decrease in mass is evident when the potential is held at its initial value. This mass decrease may be a result of loss of toluene. Also, again, a significant but much smaller mass loss is observed in the first few seconds after the potential is stepped from 0.000 V vs Ag/Ag^+ to the above-mentioned values. However, unlike the Bu_4N^+ case, subsequently, the mass rapidly increases with time, indicating the occurrence of intercalation of the smaller cations into the crystal lattice. Again, in contrast to the case for Bu_4N^+ cations, after the potential is stepped back to the initial potential, the mass remains almost constant, which suggests that these smaller cations remain trapped in the matrix of the crystals. This finding supports the conclusion based on data obtained by cyclic voltammetry that, in the presence of small Li^+, Na^+, and Ba^{2+} cations, the first redox process of the solid $C_{60}\subset L_2$ complex is chemically irreversible. Because, as will be shown later, the barium-containing reduced complex is not very soluble in acetonitrile, the decrease in mass observed after the second potential step probably corresponds to the loss of toluene (Figure 8d).

The role of the solvent must also be considered in the interpretation of EQCM data, as toluene can be lost or displaced by CH_3CN and solvated rather than nonsolvated cations can be incorporated into solid lattice upon reduction. Thus, it should

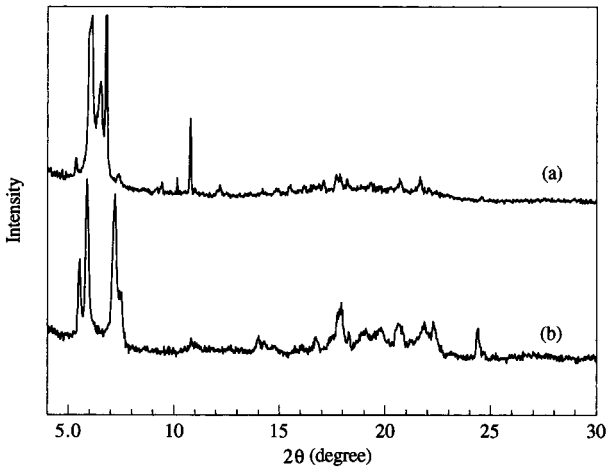

Figure 9. X-ray diffraction powder patterns obtained for crystalline C_{60}⊂L_2 complex (a) before bulk electrolysis and (b) after reduction to [C_{60}⊂L_2]$^{\bullet-}$ species. Supporting electrolyte, 0.10 mol L^{-1} Ba(ClO_4)$_2$ in CH_3CN; X-ray wavelength, 1.540 59 Å.

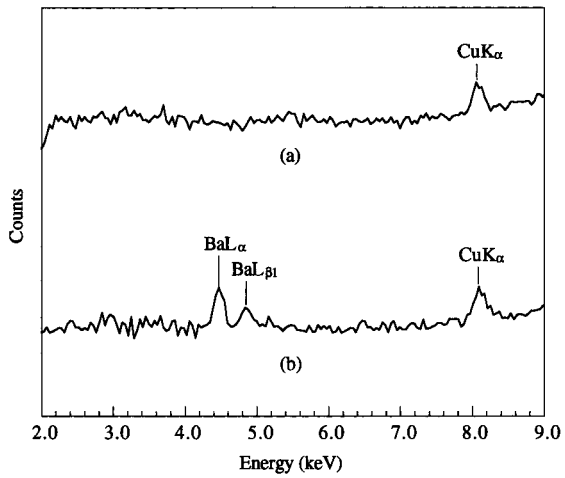

Figure 10. Energy-dispersive X-ray microanalysis obtained for crystalline C_{60}⊂L_2 (a) before bulk electrolysis and (b) after one-electron reduction to [C_{60}⊂L_2]$^{\bullet-}$ species. Supporting electrolyte, 0.10 mol L^{-1} Ba(ClO_4)$_2$/CH_3CN; accelerating voltage, 20 kV.

be noted that, except in the case of Bu_4N^+ cations (Figure 8a), the mass gains observed in the potential-step reduction (Figure 8b−d) are much larger than those calculated on the basis of an initial C_{60}⊂L_2 coverage of 7.5 ± 0.2 μg (Figure 4), even if the dissolution of a significant quantity of reduced species is neglected. The result of this calculation implies that acetonitrile (electrolyte) molecules, in addition to the small cations, may become incorporated into the lattice of the reduced complex crystals. However, such conclusions must be tentative as mass changes may also involve loss and then uptake of toluene.

X-ray Powder Diffraction and Energy-Dispersive X-ray Microanalysis of Reduced Solid [C_{60}⊂L_2]$^{\bullet-}$ Containing Ba^{2+} Cations. Solid [C_{60}⊂L_2]$^{\bullet-}$ was generated by a bulk-controlled potential electrolysis experiment in CH_3CN with 0.10 mol L^{-1} Ba(ClO_4)$_2$ as the supporting electrolyte (see Experimental Section for details). During the course of ca. 10 h of bulk electrolysis, no color change was observed in the electrolyte solution. This result also supports the hypothesis that C_{60}^- anions, which have a characteristic dark red-purple color in CH_3CN,[37] always remain complexed with the calix[5]arene. This experiment also confirms that the one-electron-reduced form of the complex has a low solubility in this medium.

Figure 9 shows the X-ray diffraction powder pattern obtained for crystalline C_{60}⊂L_2 complex before bulk electrolysis (Figure 9a) and after reduction to the [C_{60}⊂L_2]$^{\bullet-}$ species (Figure 9b). As expected, C_{60}⊂L_2 and [C_{60}⊂L_2]$^{\bullet-}$, with presumed Ba^{2+} cations to balance the charge, clearly have different solid-state structures.

Energy-dispersive X-ray microanalysis spectra confirmed the existence of barium in the structure of the [C_{60}⊂L_2]$^{\bullet-}$ crystals (Figure 10b). Importantly, no chlorine was detected, as would have been expected if Ba(ClO_4)$_2$ had become irreversibly trapped in the solid. The content of Ba^{2+} cations in the reduced crystals was estimated[38] at about 1% (wt %), which is in good agreement with the value of 1.23% calculated theoretically on the basis of the charge consumed during the course of the bulk electrolysis. The Cu Kα signal shown at 8.05 keV in Figure 10 was derived from the substrate used to support the solid and was used as an internal energy standard.

EPR Spectroscopy of Reduced Solid [C_{60}⊂L_2]$^{\bullet-}$ Containing Ba^{2+} Cations. There have been many studies describing the EPR spectroscopy of $C_{60}^{\bullet-}$ and more highly reduced anions[39] of C_{60} in solution, frozen solution, and solid-state phases. One of the characteristics on the EPR spectrum of $C_{60}^{\bullet-}$ is the low

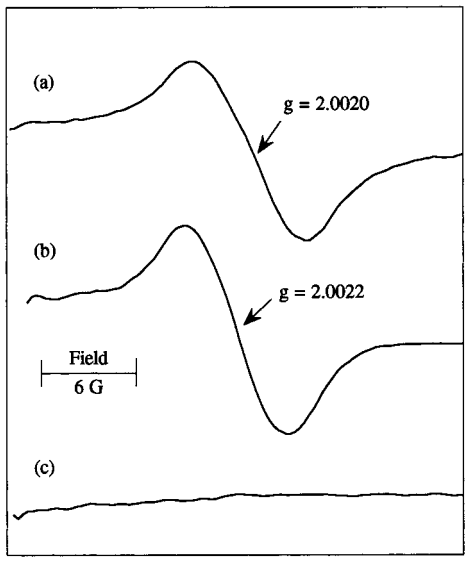

Figure 11. EPR spectra obtained for reduced solid [C_{60}⊂L_2]$^{\bullet-}$ species containing Ba^{2+} as the cation at (a) 293 K and (b) 77 K. (c) No EPR signal was found for nonreduced C_{60}⊂L_2 complex at 293 K.

g value, which is typically very close to 2.0000 and which has been attributed to spin−orbit coupling that results from Jahn−Teller distortion of the t_{1u} LUMO of C_{60}.[39b,39i,40] This *g* value is significantly smaller than the free-electron value ($g = 2.0023$) and the values for typical condensed-ring aromatic anion radicals such as naphthalene$^{\bullet-}$ ($g = 2.00276$) and perylene$^{\bullet-}$ ($g = 2.00267$).[39t] However, as indicated by Eaton et al.,[39e,39f] the *g* value is expected to be close to 2.002 if the structural distortion of $C_{60}^{\bullet-}$ provides large deviations from I_h symmetry. In the present study, each C_{60} is encapsulated by two calix[5]arene molecules, and therefore, significant distortion of the structure from I_h symmetry is expected in the reduced form of the complex.

Figure 11 shows the EPR spectra of reduced [C_{60}⊂L_2]$^{\bullet-}$ solid containing Ba^{2+} as the cation at 293 K (Figure 11a) and 77 K (Figure 11b), with *g* values of 2.0020 and 2.0022, respectively. Clearly, the measured *g* values are significantly larger than those reported previously for free $C_{60}^{\bullet-}$ radicals and much closer to the *g* values obtained for a free electron and many other organic radicals.[41] However, as noted above, this is not surprising, given that the *g* values obtained in this study reflect the properties of

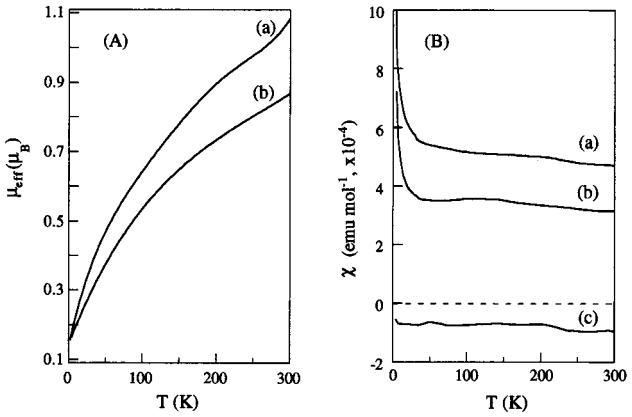

Figure 12. Magnetic susceptibility data for reduced crystalline $[C_{60}\subset L_2]^{\bullet-}$ solid containing Ba^{2+} cations. (A) magnetic moment vs temperature and (B) molar susceptibility vs temperature. (a) Prior to exposure of $[C_{60}\subset L_2]^{\bullet-}$ to the air, (b) after exposure of $[C_{60}\subset L_2]^{\bullet-}$ to the air for two weeks, and (c) nonreduced $C_{60}\subset L_2$.

complexed $[C_{60}\subset L_2]^{\bullet-}$ rather than those of simple $C_{60}^{\bullet-}$ radicals. With a decrease in temperature, the *g* value increases, as expected if more structural distortion occurs. The spectra had a peak-to-peak width of 7.2 G at 293 K, while a slightly narrower value of 6.6 G was obtained at 77 K, which is consistent with the electron hopping rate being slower at the lower temperature. As expected, no EPR signal was observed for the nonreduced $C_{60}\subset L_2$ complex (Figure 11c), as C_{60} is diamagnetic.

Magnetic Properties of Reduced Solid $[C_{60}\subset L_2]^{\bullet-}$ Containing Ba^{2+} Cations. The magnetic susceptibility of reduced crystalline $[C_{60}\subset L_2]^{\bullet-}$ containing Ba^{2+} cations was measured as a function of temperature (Figure 12). Note that the data given in Figure 12 are based on the assumption that four toluene molecules were lost from each $[C_{60}\subset L_2]\bullet$8toluene complex during the process of bulk electrolysis and that the contributions to the mass from the counterion were insignificant and ignored (molecular weight of $[C_{60}\subset L_2]\bullet$8toluene, 2787 g mol^{-1}). However, the nature of Figure 12 is independent of the number of toluene molecules. The plot of magnetic moment, μ_{eff}, versus temperature for solid $[C_{60}\subset L_2]^{\bullet-}$ (curve a of Figure 12A) continuously increased with temperature, and no characteristic plateau appeared at higher temperatures over the temperature range examined. Such behavior can be attributed to extensive delocalization of the unpaired electrons over the entire structure. The μ_{eff} value obtained at 300 K was much smaller than the 1.73 μ_B expected theoretically[42] for an $S = {}^1/_2$ state. A low value is expected on the basis of charge consumed during the bulk electrolysis, which suggests that not all of the $C_{60}\subset L_2$ complex was reduced to the $[C_{60}\subset L_2]^{\bullet-}$ species. In addition, uncertainties associated with the molar mass of the reduced solid (see above) made further discussion of this apparently low value of μ_{eff} unwarranted.

After the $[C_{60}\subset L_2]^{\bullet-}$ solid was exposed to the air, oxidation of $[C_{60}\subset L_2]^{\bullet-}$ to $C_{60}\subset L_2$ and/or some oxygen-contained species was anticipated, in which case the μ_{eff} value would decrease. However, curve b of Figure 12A shows the result of such an experiment, and surprisingly, relatively large magnetic moment values were retained even after the $[C_{60}\subset L_2]^{\bullet-}$ species had been exposed to air for a two-week period. This suggests that $[C_{60}\subset L_2]^{\bullet-}$ salts are quite stable in air, although it is possible that initially formed $[C_{60}\subset L_2]^{\bullet-}$ oxidation products could cover the surface of the unoxidized crystals and provide protection against further rapid oxidation.

The relationship between the molar susceptibility, χ, and temperature for $[C_{60}\subset L_2]^{\bullet-}$ before and after exposure to the air is displayed in curves a and b, respectively, of Figures 12. The related behavior for neutral $C_{60}\subset L_2$ crystals also is shown in curve c of Figure 12B for reference. Consistent with the data obtained from EPR spectroscopy (Figure 11c), the negative χ values clearly indicate that the $C_{60}\subset L_2$ complex is diamagnetic.

Conclusions

The electrochemical behavior of microcrystals of the $C_{60}\subset L_2$ complex adhered to electrode surfaces that are placed in acetonitrile (electrolyte) media strongly depends on the nature of the electrolyte cations used. In CH_3CN containing large Bu_4N^+ cations as the electrolyte, the voltammograms of the solid $C_{60}\subset L_2$ complex showed six successive one-electron-reduction steps, of which the first two have characteristics of being chemically reversible, while complete dissolution of the solid occurs after the third process. However, in an electrolyte containing much smaller Li^+, Na^+, or Ba^{2+} cations, even the first reduction process was chemically irreversible. Microgravimetric−double-potential-step (EQCM) experiments confirmed that the first chemically reversible/irreversible reduction process is associated with the reversible/irreversible intercalation processes of electrolyte cations into the lattice of $C_{60}\subset L_2$ crystals. Energy-dispersive X-ray microanalysis on reduced solid prepared in the presence of Ba^{2+} as the electrolyte revealed that Ba^{2+} can be injected into the solid to achieve charge neutralization during the course of the first reduction process.

The *g* values of 2.0020 ± 0.0002 at 293 K and 2.0022 ± 0.0002 at 77 K that were found for reduced solid $[C_{60}\subset L_2]^{\bullet-}$ containing Ba^{2+} cations suggest that significant distortion of the fullerene structure is present in this solid. Magnetic measurements indicate that extensive unpaired electron delocalization may occur within the structure of the reduced solid and that reduced $[C_{60}\subset L_2]^{\bullet-}$ solid is relatively stable in air.

The interactions between C_{60} and calix[5]arenes are sufficiently strong that free reduced C_{60} anions are not produced during the course of reduction, as is the case when *p-tert*-butylcalix[8]arene-C_{60} complex is reduced.[18]

Acknowledgment. The authors gratefully acknowledge the Australian Research Council for financial support of this project. B. Moubaraki (Department of Chemistry, Monash University), D. Hutton, and R. Mackie (Department of Physics, Monash University) are acknowledged for assistance with magnetic, EPR measurements, and X-ray analysis, respectively.

References and Notes

(1) Shinka, S. *Chem. Commun.* **1994**, *22*, 2586.
(2) Williams, R. M.; Verhoeven, J. M. *Recl. Trav. Chim. Pay-Bas.* **1992**, *111*, 531.
(3) Atwood, J. L.; Koustantonic, G. A.; Raston, C. L. *Nature* **1994**, *368*, 229.
(4) Suzuki, T.; Nakashima, K.; Shinkai, S. *Chem. Lett.* **1994**, 699.
(5) Chen, Z.; Fox, J. M.; Gale, P. A.; A. J., P.; Beer, P. D.; Rosseinsky, M. J. *J. Electroanal. Chem.* **1995**, *392*, 101.
(6) Williams, R. M.; Zwier, J. M.; Verhoeven, J. W.; Nachtegoal, G. H.; Kentgens, A. P. M. *J. Am. Chem. Soc.* **1994**, *116*, 6965.
(7) Castillo, R.; Ramos, S.; Cruz, R.; Martinez, M.; Lara, F.; Ruiz-Garcia, J. *J. Phys. Chem.* **1996**, *100*, 709.
(8) Suzuki, T.; Nakashima, K.; Shinkai, S. *Tetrahedron Lett.* **1995**, *36*, 249.
(9) Isaacs, N. S.; Nichols, P. J.; Raston, C. L.; Sandoval, C. A.; Young, D. J. *Chem. Commun.* **1997**, 1839.
(10) Raston, C. L.; Atwood, J. L.; Nichols, P. J.; Sudria, I. B. N. *Chem. Commun.* **1996**, 2615.
(11) Raston, C. L. *Chem. Austr.* **1997**, 12.
(12) Atwood, J. L.; Barbour, L. J.; Nichols, P. J.; Raston, C. L.; Sandoval, C. A. *Chem. Eur. J.* **1999**, *5*, 990.
(13) Diederich, F.; Rubin, Y. *Angew. Chem., Int. Ed. Engl.* **1992**, *31*, 1101.
(14) Taylor, R.; Walton, D. R. M. *Nature* **1993**, *363*, 685.
(15) Baum, H. R. M. *Chem. Eng. News* **1993**, *71* (47), 8.

(16) Friendman, S. H.; DeCamp, D. L.; Sijbesma, R. P.; Srdanov, G.; Wudl, F.; Kenyon, G. *J. Am. Chem. Soc.* **1993**, *115*, 6506.
(17) Li, N. Q.; Zhou, B.; Luo, H. X.; He, W. J.; Shi, Z. J.; Gu, Z. N.; Zhou, X. H. *J. Solid State Electrochem.* **1998**, *2*, 253.
(18) Cliffel, D. E.; Bard, A. J.; Shinkai, S. *Anal. Chem.* **1998**, *70*, 4146.
(19) Olsen, S. A.; Bond, A. M.; Compton, R. G.; Lazarev, G.; Mahon, P. J.; Marken, F.; Raston, C. L.; Tedesco, V.; Webster, R. D. *J. Phys. Chem. A* **1998**, *102*, 2641.
(20) Hardie, M. J.; Raston, C. L. *Chem. Commun.* **1999**, 1153.
(21) Gutsche, C. D. *Calixarenes*; The Royal Society of Chemistry: Cambridge, U.K., 1989.
(22) Grote Gansey, M. H. B.; Verboom, W.; Reinhoudt, D. N. *Tetrahedron. Lett.* **1994**, *35*, 7127.
(23) *Calixarenes. A Versatile Class of Macrocyclic Compounds*; Vicens, J., Böhmer, V., Eds.; Kluwer: Dordrecht, Germany, 1991.
(24) Danil de Namor, A. F.; Pardo, M. T. G.; Tanaka, D. A. P.; Velarde, F. S. S.; Garcia, J. D. C.; Cabaleiro, M. C.; Al-Rawi, J. M. A. *J. Chem. Soc., Faraday Trans.* **1993**, *89*, 2727.
(25) Danil de Namor, A. F. *Pure Appl. Chem.* **1993**, *65*, 193.
(26) Shi, Y.; Zhang, Z. *Chem. Commun.* **1994**, 375.
(27) Ruoff, R. S.; Tse, D. S.; Malhotra, R.; Lorents, D. C. *J. Phys. Chem.* **1993**, *97*, 3379.
(28) Bond, A. M.; Miao, W. J.; Raston, C. L. *J. Phys. Chem. B* **2000**, *104*, 2320.
(29) Webster, R. D.; Bond, A. M.; Schmidt, T. *J. Chem. Soc., Perkin Trans. 2* **1995**, 1365.
(30) Suarez, M. F.; Marken, F.; Compton, R. G.; Bond, A. M.; Miao, W.; Raston, C. L. *J. Phys. Chem. B* **1999**, *103*, 5637.
(31) Bond, A. M.; Oldham, K. B.; Miao, W. J.; Feldberg, S. W.; Raston, C. L. In *Sixth International Seminar on Electroanalytical Chemistry (Extended Abstracts)*; Chinese Chemical Society: Changchun, China, 1997; p 77.
(32) Cliffel, D. E.; Bard, A. J. *J. Phys. Chem.* **1994**, *98*, 8140.
(33) Chlistunoff, J.; Cliffel, D.; Bard, A. J. *Thin Solid Films* **1995**, *257*, 166.
(34) Compton, R. G.; Spackman, R. A.; Riley, D. J.; Wellington, R. G.; Eklund, J. C.; Fisher, A. C.; Green, M. L. H.; Doothwaite, R. E.; Stephens, A. H. H.; Turner, J. *J. Electroanal. Chem.* **1993**, *344*, 235.
(35) Compton, R. G.; Spackman, R. A.; Wellington, R. G.; Green, M. L. H.; Turner, J. *J. Electroanal. Chem.* **1992**, *327*, 337.
(36) Heslop, R. B.; Jones, K. *Inorganic Chemistry, A guide to advanced study*; Elsevier Scientific Publishing Company: New York, 1976.
(37) Dubois, D.; Moninot, G.; Kutner, W.; Jones, T. M.; Kadish, K. M. *J. Phys. Chem.* **1992**, *96*, 7137.
(38) Goldstein, J. I.; Newbury, D. E.; Echlin, P.; Joy, D. C.; Romig, J. A. D.; Lyman, C. E.; Fiori, C.; Lifshin, E. *Scanning Electron Microscopy and X-ray Microanalysis*, 2nd ed.; Plenum Press: New York, 1992.
(39) (a) Dubois, D.; Kadish, K. M.; Flanagan, S.; Haufler, R. E.; Chibante, L. P. F.; Wilson, L. J. *J. Am. Chem. Soc.* **1991**, *113*, 4363. (b) Greaney, M. A.; Gorun, S. M. *J. Phys. Chem.* **1991**, *95*, 7142. (c) Dubois, D.; Jones, M. T.; Kadish, K. M. *J. Am. Chem. Soc.* **1992**, *114*, 6446. (d) Schell-Sorokin, A. J.; Mehran, F.; Eaton, G. R.; Eaton, S. S.; Viehbeck, A.; O'Toole, T. R.; Brown, C. A. *Chem. Phys. Lett.* **1992**, *195*, 225. (e) Khaled, M. M.; Carlin, R. T.; Trulove, P. C.; Eaton, G. R.; Eaton, S. S. *J. Am. Chem. Soc.* **1994**, *116*, 3465. (f) Easton, S. S.; Kee, A.; Konda, R.; Eaton, G. R.; Trulove, P. C.; Carlin, R. T. *J. Phys. Chem.* **1996**, *100*, 6910. (g) Easton, S. S.; Easton, G. R. *Appl. Magn. Reson.* **1996**, *11*, 155. (h) Kato, T.; Kodama, T.; Oyama, M.; Okazaki, S.; Shida, T.; Nakagawa, T.; Matsui, Y.; Suzuki, S.; Shiromaru, H.; Yamauchi, K.; Achiba, Y. *Chem. Phys. Lett.* **1991**, *186*, 35. (i) Kato, T.; Kodama, T.; Shida, T. *Chem. Phys. Lett.* **1993**, *205*, 405. (j) Stinchcombe, J.; Penicaud, A.; Bhyrappa, P.; Boyd, P. D. W.; Reed, C. A. *J. Am. Chem. Soc.* **1993**, *115*, 5212. (k) Boyd, P. D. W.; Byrappa, P.; Paul, P.; Stinchcombe, J.; Bolskar, R. D.; Sun, Y.; Reed, C. A. *J. Am. Chem. Soc.* **1995**, *117*, 2907. (l) Sun, Y.; Reed, C. A. *Chem. Commun.* **1997**, 747. (m) Sun, Y.; Drovetskaya, T.; Bolskar, R. D.; Bau, R.; Boyd, P. D.; Reed, C. A. *J. Org. Chem.* **1997**, *62*, 3642. (n) Moriyama, H.; Kobayashi, H.; Kobayashi, A.; Watanabe, T. *J. Am. Chem. Soc.* **1993**, *115*, 1185. (o) Hwang, Y. L.; Yang, C. C.; Hwang, K. C. *J. Phys. Chem.* **1997**, *101*, 7971. (p) *Recent Advances in the Chemistry and Physics of Fullerenes and Related Materials*; Kadish, K. M., Rouff, R. S., Eds.; The Electrochemical Society: Pennington, NJ, 1994. (q) Stasko, A.; Brezova, V.; Rapta, P.; Dinse, K. P. *Fullerene Sci. Technol.* **1996**, *5*, 593. (r) Stasko, A.; Brezova, V.; Biskupic, S.; Dinse, K. P.; Gross, R.; Baumgarten, M.; Gugel, A.; Belik, P. *J. Electroanal. Chem.* **1997**, *423*, 131. (s) Kukolich, S. G.; Huffman, D. R. *Chem. Phys. Lett.* **1991**, *182*, 263. (t) Misra, S. K.; Petkov, V. *Appl. Magn. Reson.* **1995**, *8*, 277. (u) Tumanskii, B. L. *Russ. Chem. Bull.* **1996**, *45*, 2267. (v) Kitajima, Y.; Miyamoto, Y.; Matsuura, K.; Hase, H. *Chem. Lett.* **1999**, 237. (w) Hase, H.; Miyatake, Y. *Chem. Phys. Lett.* **1994**, *229*, 593. (x) Hase, H.; Miyatake, Y. *Chem. Phys. Lett.* **1995**, *245*, 95. (y) Khairulin, I. I.; Chang, W. T.; Hwang, L. P. *Fullerene Sci. Technol.* **1996**, *4*, 423.
(40) Allemand, P. M.; Koch, A.; Wudl, F.; Rubin, Y.; Diederich, F.; Alvarez, M. M.; Anz, S. J.; Whetten, R. L. *J. Am. Chem. Soc.* **1991**, *113*, 1050.
(41) Raymond, S. A. *Electron Paramagnetic Resonance*; John Wiley & Sons: New York, 1968.
(42) Bhyrappa, P.; Paul, P.; Stinchcombe, J.; Boyd, P. D. W.; Reed, C. A. *J. Am. Chem. Soc.* **1993**, *115*, 11004.